THE OFFICIAL MAGAZINE OF THE OCEANOGRAPHY SOCIETY

Oceanography

CAPTURING FRESH LAYERS
WITH THE SURFACE SALINITY PROFILER

By Kyla Drushka,
William E. Asher,
Andrew T. Jessup,
Elizabeth J. Thompson,
Suneil Iyer,
and Dan Clark

ABSTRACT. During the second Salinity Processes in the Upper-ocean Regional Study (SPURS-2) field experiments in 2016 and 2017 in the eastern tropical Pacific Ocean, the surface salinity profiler (SSP) measured temperature and salinity profiles in the upper 1.1 m of the ocean. The SSP captured the response of the ocean surface to 35 rain events, providing insight into the generation and evolution of rain-formed fresh layers. This paper describes the measurements made with the SSP during SPURS-2 and quantifies the fresh layers in terms of their vertical salinity gradients between 0.05 m and 1.1 m, $\Delta S_{1.1-0.05m}$. For the 35 rain events sampled with the SSP in 2016 and 2017, the maximum value of $\Delta S_{1.1-0.05m}$ is well correlated with the accumulated rainfall. The maximum value of $\Delta S_{1.1-0.05m}$ is shown to be linearly proportional to the maximum rain rate and inversely proportional to the wind speed. This wind speed-dependent relationship shows a high degree of scatter, reflecting that the vertical salinity gradient formed during any individual rain event depends on the complex interaction between the local ocean dynamics and the highly variable forcing from rain and wind.

Photo credit: Dan Clark, Applied Physics Laboratory, University of Washington

INTRODUCTION

Frequent rainfall helps to maintain the relatively fresh (~33 psu) surface waters beneath the Intertropical Convergence Zone (ITCZ) of the eastern tropical Pacific Ocean. Rain cells on scales of O(1 to 100) km within the ITCZ episodically deposit freshwater onto the ocean surface, producing buoyant fresh layers that are eventually integrated into the underlying ocean through advection and mixing. One of the major objectives of the second Salinity Processes in the Upper-ocean Regional Study (SPURS-2) experiment is to understand the generation and evolution of rain-formed fresh layers, including the spatial and temporal scales of their salinity anomalies (defined in terms of the surface freshening observed by satellites). As part of the SPURS-2 experiment, we made measurements of temperature, salinity, and turbulent dissipation rate in the upper meter of the ocean at fine horizontal, vertical, and temporal resolution using the surface salinity profiler (SSP; Asher et al., 2014a,b), a surface-following platform that is towed from a ship. These data will enable us to characterize the structure of near-surface fresh layers formed by rain. In this article, we focus on the salinity response of the upper ocean to rain.

Although it is known that the strongest impact of rain occurs in the upper tens of centimeters of the ocean, few observations of salinity have been made over these shallow depths due to difficulties in sampling close to the ocean surface. Therefore, much of our detailed knowledge about the impacts of rainfall on the upper meter of the ocean comes from laboratory experiments (Ho et al., 2004; Zappa at al., 2009; Harrison et al., 2012) and modeling (Soloviev et al., 2015; Drushka et al., 2016; Bellenger et al., 2016). These studies have been supplemented by a limited number of field observations that have characterized rain impacts on the upper few meters of the ocean surface (e.g., Price et al., 1979; Soloviev and Lukas, 1997; Wijesekera et al., 1999; Asher et al., 2014a; Walesby et al., 2015; Moulin et al., 2018; Thompson et al., 2019; ten Doeschate et al., in press). The consistent results from these laboratory, modeling, and field studies indicate that rainfall forms layers of stably stratified fresher water on the order of 1 m to 10 m thick at the ocean surface, and that these "fresh layers" can persist from minutes to hours, depending on ocean surface mixing due to wind forcing, convective overturning, and internal and surface waves.

The impact of rainfall on the ocean is often characterized in terms of the vertical salinity gradient, ΔS_{Z2-Z1}, between depths Z_1 and Z_2. As an example, salinity measurements from the Soil Moisture and Ocean Salinity (SMOS) or Aquarius satellite products, with a radiometric measurement depth of approximately 0.01 m, have been compared with salinity measured at 5 m by Argo profiling floats. The difference in salinity from these platforms gives $\Delta S_{5-0.01\mathrm{m}}$, the vertical gradient in salinity between 0.01 m and 5 m depth. Several studies have determined that in the tropics there is a linear relationship between $\Delta S_{5-0.01\mathrm{m}}$ and the local rain rate (R):

$$\Delta S_{1.1-0.05\mathrm{m}} = kR, \qquad (1)$$

where $\Delta S_{5-0.01\mathrm{m}} > 0$ indicates fresher values at 0.01 m compared to 5 m and R is provided by satellite-derived rain products (e.g., Boutin et al., 2014; Drucker and Riser, 2014; Santos-Garcia et al., 2014). Depending on the satellite data products used for salinity and rain, values for k ranging from 0.07 to 0.36 psu $(\mathrm{mm\ hr^{-1}})^{-1}$ have been estimated (see Boutin et al., 2016, for a review of these studies).

Equation 1 does not take into account other parameters that have been found to influence the formation of salinity gradients. For instance, wind can affect salinity gradients by generating turbulence that mixes the ocean surface (Asher et al., 2014a; Thompson et al., 2019; ten Doeschate et al., in press). Drushka et al. (2016) used a one-dimensional model to explore the influence of both rain rate and wind speed on vertical salinity gradients for idealized rain events having constant wind speed and a Gaussian-shaped rain rate time series. Similar to Equation 1, they found that

$$\Delta S_{5-0.05\mathrm{m}} = kR_{max}U_{10}{}^{-b}, \qquad (2)$$

where U_{10} is the wind speed at a height of 10 m, R_{max} is the maximum rain rate during the event, $k = 0.11$ psu $(\mathrm{mm\ hr^{-1}})^{-1}$, and $b = 1.1$. Equations 1 and 2 are not equivalent: for $2 \le U_{10} \le 10\ \mathrm{m\ s^{-1}}$ and $1 \le R_{max} \le 100\ \mathrm{mm\ hr^{-1}}$, $\Delta S_{5-0.01\mathrm{m}}$ calculated using Equation 2 is an order of magnitude smaller than that predicted from fits of satellite/Argo data to Equation 1. The cause of this difference is unclear, but possible explanations are that a one-dimensional model may not fully account for all the processes governing fresh layer dynamics, or that differences in the spatiotemporal scales of satellite measurements (which are averaged in space and time) and the model (which represents a point measurement) could lead to the differences in the estimations of ΔS. There are also other factors not represented in Equation 2 that may be important for predicting vertical salinity gradients (e.g., preexisting surface ocean stratification, air-sea heat fluxes, mixing from surface and internal waves).

The objective of data collection with the SSP during SPURS-2 was to systematically characterize near-surface salinity, temperature, and turbulence within rain-formed fresh layers over a range of oceanic and atmospheric conditions. In this paper, we focus on the salinity and temperature measurements made from the SSP; detailed discussion of the microstructure turbulence measurements will be presented in a forthcoming study. The SSP measurements are used to quantify vertical salinity gradients within fresh layers, including their relationship to rain and wind forcing. The observations are also used to validate and reconcile the parameterizations in Equations 1 and 2.

DATA

The Surface Salinity Profiler

The SSP samples temperature and salinity in the upper meter of the ocean while being towed from a ship, as described by

Asher et al. (2014a,b). The SSP used for SPURS-2 was a second-generation platform whose modified design provided additional capabilities. The modified SSP consisted of a 3.8 m long, 0.74 m wide, 0.13 m thick stand-up paddleboard attached with two horizontal struts to a 2.2 m long surfboard that was located inboard of the paddleboard relative to the ship. The paddleboard provided the majority of the buoyancy, while the surfboard acted as a stabilizing outrigger (Figure 1a). A 1.2 m deep by 0.6 m wide keel was affixed to the bottom of the center of the paddleboard and was secured to the outrigger with angled struts in order to reduce vibration of the instrumented keel and increase the strength of the SSP (Asher et al., 2014b). The keel of the SSP was constructed from a 12.5 mm thick layer of rubber sandwiched between 3 mm thick aluminum plates to further isolate sensors from vibration while the platform was towed.

Four CTD sensors (SBE 49, Sea-Bird Electronics) were mounted to the keel at depths of 0.12, 0.23, 0.54, and 1.10 m below the ocean surface. Salinity in the upper 0.05 m was measured using a "salinity snake" that pumped water from a floating hose with an intake depth in the upper 0.05 m through a vortex debubbler and then a thermosalinograph (TSG; SBE 45, Sea-Bird Electronics). Seawater temperature at the intake of the salinity snake was measured using a self-logging temperature sensor (SBE 56, Sea-Bird Electronics) that was mounted on the intake hose (Figure 1a shows the articulated arm used for the 2017 field experiments that held the SBE 56 and intake hose for the salinity snake). Each CTD was sampled at 6 Hz, the TSG was sampled at 2 Hz, and the SBE 56 logged temperature at 1 Hz.

The SSP also measured the microstructure temperature and conductivity using probes (MicroSquid, Rockland Scientific) that were mounted to the SSP keel at 0.37 m depth below the water line. The microstructure probes were mounted on opposite sides of the keel, with each sensing element located forward of the CTD intakes in order to avoid flow distortion. In 2017, a downward-looking Nortek Vectrino-II profiling acoustic Doppler velocimeter (ADV) was mounted on the keel at 0.5 m depth and a downward-looking Nortek Signature1000 acoustic Doppler current profiler (ADCP) was mounted outboard of the paddleboard at a depth of 0.1 m. The ADCP operated in high-resolution mode and measured velocities in 0.02 m vertical bins from 0.2 m to 2 m depth below the sea surface. An inertial measurement unit took data that allowed platform motion to be decoupled from the ADV and ADCP velocity records.

The SSP was deployed episodically for up to 12 hours per deployment, with 18 deployments during the 2016 cruise and 16 during the 2017 cruise. During each deployment, the SSP provided a continuous record of temperature and salinity from 0.05 m to 1.1 m depth, along with measurements of turbulence from 0.2 m to 2 m. The SSP was towed from a point near the center of the ship on the port side using a 50 m long tow cable attached to a three-point bridle system, which forced it to track at a ~135° angle relative to the ship's heading. As a result, the SSP was 35 m outboard and 10 m aft of the vessel, thus sampling water undisturbed by the ship's wake (Figure 1b; Asher et al., 2014a,b). The SSP was towed at a maximum speed of 2 m s^{-1} in order to minimize bubble generation by the platform and to provide a reasonable balance between resolution of large- and small-scale horizontal features in the ocean. At this speed, the SSP followed the water level over swell and non-breaking wind waves such that the instruments maintained approximately the same depth below the sea surface. This was confirmed by the 0.02 m root-mean-square variance in the pressure data from the keel-mounted CTDs.

Salinity data from the CTDs mounted at 0.12 m and 0.23 m were processed to remove spikes (caused by bubbles) by computing a moving median and standard deviation over non-overlapping

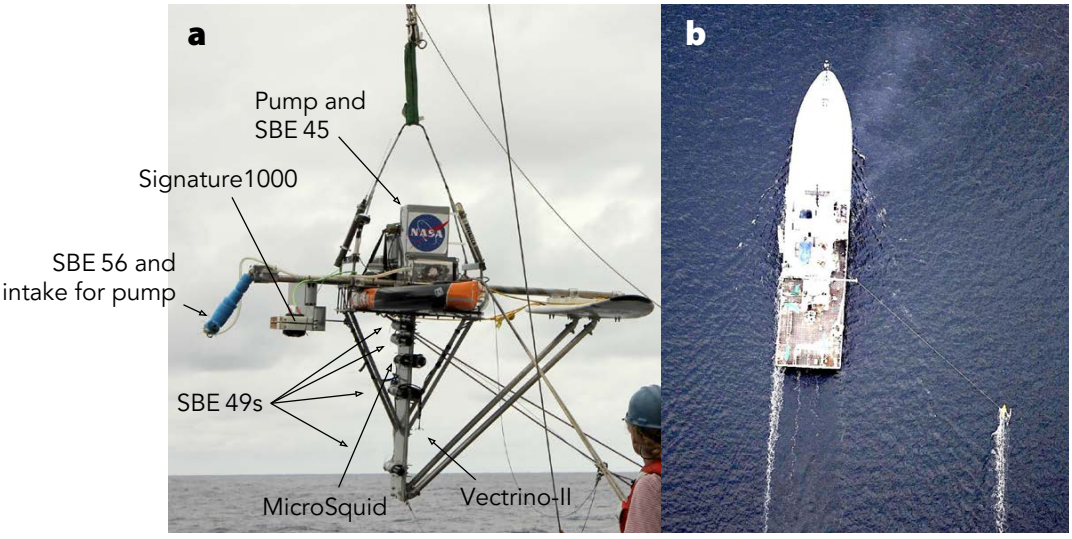

FIGURE 1. Surface salinity profiler (SSP). (a) Front view of the SSP (2017 version) with instruments labeled. (b) Aerial view of SSP being towed from a research vessel (ship length is 84 m); note that the SSP is outside of the ship's wake. In the 2016 deployments, the SSP did not include the Signature1000 or Vectrino-II, and the SBE 56 and pump intake were mounted to hoses that dragged in the water rather than on the sampling "arm" shown here.

two- to five-minute data segments. The median salinity was subtracted from each data segment to isolate the salinity deviations, and data points in the original time series for which the corresponding value of the deviations were more than three times larger than the standard deviation were masked out. Missing data points were then filled either with linear interpolation if the missing value existed between two valid points or with a moving median of non-masked points taken from within the original segment of data. Salinity and temperature data at all depths were then smoothed with a 30-second moving median filter. Offsets and drift between each sensor were small, typically <0.001 psu for salinity and 0.008°C for temperature over the course of a 12-hour deployment. Mean differences in salinity and temperature between the CTDs, TSG, and SBE 56 were removed by selecting a time range for which the upper meter was well mixed (typically during night, or in non-rainy conditions with wind speed greater than 8 m s^{-1}) and correcting mean values from all sensors to those of the CTD mounted at 0.54 m depth as a reference since it was shown to be the most stable sensor.

Other Observations

The upper-ocean measurements were complemented by a suite of ship-based measurements made continuously from R/V *Revelle*. These included rain rate and wind speed (Clayson et al., 2019, in this issue), water temperature and salinity from the ship's TSG that sampled water from a nominal depth of 5 m, and ocean currents at 20 m depth and below from the ship's ADCP (provided by Janet Sprintall, Scripps Institution of Oceanography). An Eigenbrodt ODM470 optical disdrometer was also deployed on the ship to measure raindrop size distributions. The meteorological sensors on the ship's bow were approximately 90 m forward of the SSP's position. At 2 m s^{-1} ship speed, this introduced a 45 s lag between the meteorological and SSP observations. All SSP measurements were thus offset by 45 s in time in order to account for this lag.

In this paper, we also use satellite-based rain estimates from IMERG (Integrated Multi-satellitE Retrievals for GPM, the NASA Global Precipitation Mission; Sun et al., 2018), which are available at 10 km horizontal resolution every 30 minutes.

Sampling Considerations

Sampling data from a moving platform in principle allowed us to capture the spatial structure of the response of the ocean to rain. However, the rain cells moved continuously (approximately with the atmospheric mean flow, which was typically faster than the ship speed) and evolved (on timescales as short as 60 s). Moreover, rainwater that was deposited on the ocean surface could then be advected horizontally by currents. Thus, the SSP observations represent the impact of the rain field, which moved and evolved, on the ocean surface, which also moved and evolved. The SSP measured the vertical distribution of salinity and temperature in a particular water parcel, and the ship measured the rain rate and wind speed that occurred over the parcel at the same time. However, the vertical temperature and salinity profiles of a given parcel also depended on the rain and wind speed history for that parcel, the details of which are not always known. As a result, correlating a salinity profile observed with the SSP to rain rates and wind speeds measured from the ship requires a cautious approach. Here, we assume that one-dimensional vertical processes (surface forcing, vertical mixing) dominated the oceanic response to rain forcing, so that over the timescales of the evolving rain field, the fresh layer evolved in the vertical direction faster than the lateral dispersion occurred. We also explore different metrics to describe rain forcing and predict the response of salinity to this forcing: the maximum rain rate of an event, the total accumulated rainfall during an event, and the instantaneous rain rate at any given time.

SSP MEASUREMENTS OF NEAR-SURFACE SALINITY

During the two SPURS-2 cruises, the SSP was deployed for a total of 230 hours, of which 39 hours were characterized as having local rain rates above 0.5 mm hr^{-1}. Within those 39 hours, 35 distinct rain events were identifiable: 15 in 2016 and 20 in 2017. Here, we define a rain event as having (1) a rain rate, R, greater than 0.5 mm hr^{-1} for at least five minutes, and (2) a $\Delta S_{1.1-0.05m}$ greater than 0.01 psu within ±15 minutes of the peak rain rate. The set of rain events spans a range of rain and wind conditions, with a median R of 11 mm hr^{-1} and a median duration of 27 minutes (Figure 2a,b). The associated wind speeds (adjusted to 10 m assuming neutral stability), U_{10}, ranged from 2 m s^{-1} to 11 m s^{-1}, with a median value of 5 m s^{-1} (Figure 2c). Although not shown here, R was not correlated with U_{10} so that

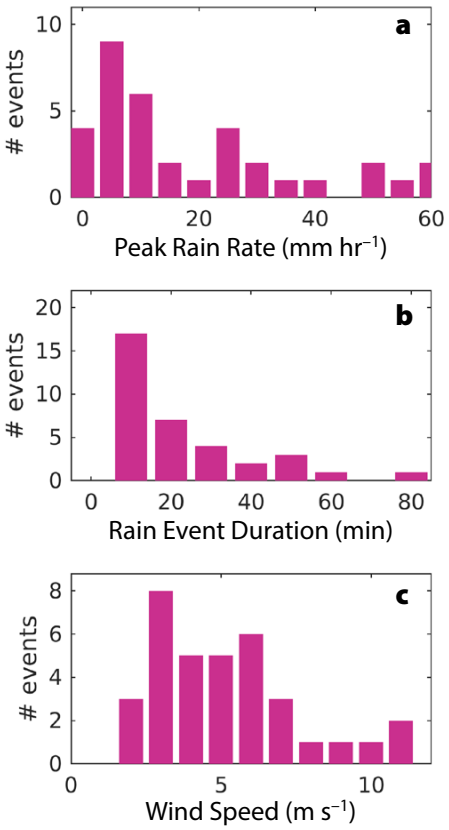

FIGURE 2. Statistics for the 35 rain events encountered while the SSP was deployed in 2016 and 2017. (a) Maximum rain rate during the events. (b) Duration of the events, defined as the total number of raining minutes. (c) Average wind speed during the raining minutes.

the set of observed events allows investigation into how different rain and wind combinations affect the ocean salinity response to rainfall.

Example Rain Event

Figure 3 shows time series for R, raindrop size distribution, U_{10}, current speed at 20 m depth, salinity (S), temperature (T), and turbulent dissipation rate (ε) for one rain event sampled by the SSP. In this case, the SSP was being towed south-southwestward at 2 m s^{-1}, and both the wind and current were from the north-northwest (Figure 3f). Before the rain began, the upper 5 m of the ocean were well mixed in temperature and salinity (Figure 3c,d). The rain event began at 15:33 UTC and had a maximum R, R_{max}, of 4 mm hr^{-1} at 15:37 UTC. A smaller local peak in R of 1 mm hr^{-1} occurred at 15:45 UTC, and rain ceased at 15:58 UTC. The majority of raindrops had diameters less than 0.6 mm, and drops with diameter >1 mm were only observed when R >1 mm hr^{-1} (i.e., when R was maximum for this event; Figure 3a). Wind speed dropped from 4.5 m s^{-1} to 2.3 m s^{-1}, then increased again to 4.7 m s^{-1} after the time that R_{max} occurred (Figure 3b).

The rain event generated freshening at all depths: the salinity anomaly followed the rain rate closely, with a

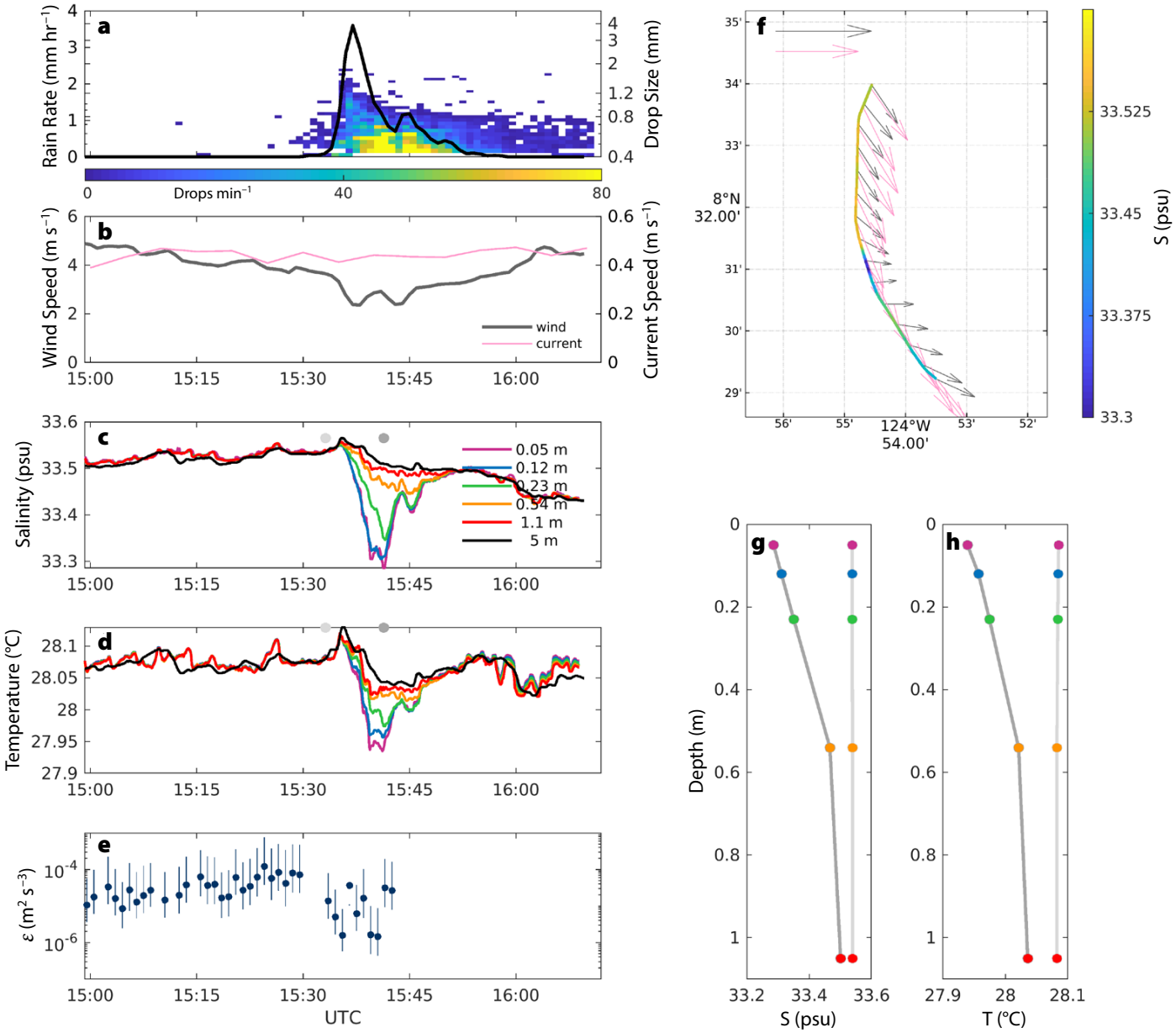

FIGURE 3. Rain event sampled with the SSP on October 31, 2017. (a) Rain rate (black line, left axis) and number of drops of a given raindrop class size per minute (color, right axis) as measured by the disdrometer. (b) Wind speed (left axis) and current speed (right axis) measured from the ship. (c) Salinity and (d) temperature measured by the SSP and the ship's thermosalinograph. (e) Dissipation rate at 0.37 m as derived from the microstructure conductivity sensor, with uncertainty bounds. (f) $S_{0.05m}$ (color) along the SSP track, with wind vectors (gray arrows; scale arrow at top is 10 m s^{-1}) and current vectors (pink vectors; scale arrow is 0.5 m s^{-1}). Vertical profiles of (g) salinity and (h) temperature from the SSP at 15:33 (light gray) and 15:41 (dark gray) UTC; these times are indicated as gray dots on panels c and d.

lag of several minutes (Figure 3c). After the rain started at 15:33 UTC, $S_{0.05m}$ decreased by 0.27 psu from 15:35 to 15:41 UTC. At 15:41 UTC, four minutes after the time that R_{max} occurred, $S_{0.05m}$ reached a minimum; immediately following this minimum, $S_{0.05m}$ increased by 0.16 psu. Following the second peak in R at 15:45 UTC, $S_{0.05m}$ decreased again by 0.04 psu, reaching a local minimum at 15:45 UTC (Figure 3c). From the time the rain started until 15:39 UTC, $S_{0.05m}$ and $S_{0.12m}$ were nearly equal, suggesting that the rainwater mixed instantaneously down to at least 0.12 m. This is consistent with laboratory experiments showing that turbulence generated by raindrops impacting on the surface penetrates to a depth of approximately 0.1 m and mixes this near-surface layer instantaneously (Zappa et al., 2009). Deeper than 0.12 m, the salinity anomalies were weaker and slightly lagged compared to $S_{0.05m}$ and $S_{0.12m}$. For instance, $S_{0.23m}$ had a maximum decrease of 0.21 psu at 15:41 UTC, whereas $S_{1.1m}$ had a maximum decrease of 0.08 psu at 15:43 UTC. S_{5m} measured by the ship's TSG showed a maximum freshening of 0.07 psu at 15:51 UTC, indicating that the rainwater penetrated to at least 5 m depth (Figure 3c). After 15:54 UTC, a 0.07 psu freshening occurred at all depths. At this time, no local R was measured and no vertical S gradient was observed, suggesting that the fresh signal was measured when the SSP crossed a front. For instance, an earlier rain event could have caused freshening in that location and the subsequent mixing could have eroded the salinity stratification, leading to a horizontal salinity front but no vertical S gradient.

Figure 3d shows that T decreased in concert with the observed decrease in S at all depths. $T_{0.05m}$ decreased by 0.19°C between 15:35 and 15:41 UTC; T_{5m} decreased by 0.08°C between 15:35 and 15:44 UTC. This rain-induced cooling is expected: the near-surface air is typically cooler than the ocean surface in the tropics, and raindrops are 1°–2°C cooler than the air (Gosnell et al., 1995), so raindrops tend to cool the ocean. As seen in salinity, T at all levels decreased again at 15:54 UTC, which is consistent with the SSP crossing a front.

The vertical profiles of S and T show that the maximum rain-induced freshening and cooling signals seen at 15:41 UTC were both strongest above 0.54 m (Figure 3g,h), indicating the formation of a thin (<0.54 m thick) stratified layer at the surface. Although measurements of ε are unavailable after 15:43 UTC, it appears that ε at 0.37 m decreased after the rain started, for example, at 15:41 UTC when the vertical stratification was strongest. It is possible that this reduction in turbulence occurred because kinetic energy from the wind stress was trapped within the stratified near-surface layer above the depth of the microstructure sensors.

Statistical Characterization of All Rain Events

The case study shown in Figure 3 is one example of the 35 rain events observed with the SSP during SPURS-2. To characterize all of the rain events and evaluate the parameterizations in Equations 1 and 2, several metrics have been defined. For each event, R_{max} was identified as the peak rain rate, and the total amount of accumulated rainfall during each rain event, ΣR, was computed. R_{IMERG} was estimated as the value of R from the IMERG satellite product within ±30 minutes of the time that R_{max} occurred, in the pixel that the SSP was in. The strength of the rain-induced salinity anomaly was defined as the maximum value of $\Delta S_{1.1-0.05m}$ within ±15 minutes of when R_{max} occurred, and is referred to as ΔS_{max}. Similarly, ΔT_{max} was defined as the maximum value of $\Delta T_{1.1-0.05m}$ within ±15 minutes of the time that R_{max} occurred. In order to capture the wind forcing affecting the development of ΔS_{max}, $\overline{U_{10}}$ was defined as the mean value of U_{10} over the time period spanning when R_{max} and ΔS_{max} occurred. By definition, this time lag between R_{max} and ΔS_{max} was <15 minutes; for the 35 rain events, it had a mean value of 3 minutes; that is, the peak vertical salinity gradient was generally observed within a few minutes of the peak rain rate.

Figure 4 summarizes the various metrics used to quantify the rain, wind, and vertical salinity gradients for the rain events observed with the SSP. Least-squares linear regressions to Equations 1 and 2 were fit to these data in order to evaluate those relationships. Table 1 summarizes the results of the fits, and includes the coefficients and their standard errors as well as the coefficient of determination (r^2) for each fit. Figure 4a shows a scatterplot of ΔS_{max} versus R_{max}, where the points have been sorted into two classes based on wind speed: $\overline{U_{10}} > 5$ m s^{-1} and $\overline{U_{10}} \leq 5$ m s^{-1}. Although considerable scatter exists in the data, it is evident that higher R_{max} and lower $\overline{U_{10}}$ are associated with larger ΔS_{max}. A least-squares linear regression between ΔS_{max} and R_{max} (Equation 1) produced a regression coefficient of $k = 0.005$ psu (mm hr^{-1})$^{-1}$ (Table 1). This value is over an order of magnitude smaller than the range of k shown in the review by Boutin et al. (2016) (from 0.07 to 0.36 psu (mm hr^{-1})$^{-1}$). However, there are two major differences between the studies summarized by Boutin et al. (2016) and the present work: differences in measurement resolution and differences in the depths over which ΔS was calculated. First, the results shown by Boutin et al. (2016) were based on satellite-derived rain products, which have coarse resolution in space and time. The coarse satellite rain measurements have lower values than the in situ rain rates measured at the ship. This discrepancy is typical over tropical oceans where much of the precipitation falls from small-scale convective events with short duration and high intensity (e.g., Houze et al., 2015). Indeed, a scatterplot of ΔS_{max} versus R_{IMERG} demonstrates that the values of R_{IMERG} are an order of magnitude lower than the R_{max} observed at approximately the same time and place (Figure 4a). The least-squares linear regression coefficient between ΔS_{max} and R_{IMERG} is $k = 0.03$ psu (mm hr^{-1})$^{-1}$ (Table 1), which is closer to the mini-

mum value of k shown by Boutin et al. (2016) than the value of k estimated with in situ R_{max}.

Second, Boutin et al. (2016) considered $\Delta S_{5-0.05m}$, while this study considers $\Delta S_{1.1-0.05m}$. Although not plotted here, the regression of ΔS_{max} to R_{IMERG}, where ΔS_{max} was computed from $\Delta S_{5-0.05m}$ (with S_{5m} measured by the ship's TSG), produced a coefficient k = 0.16 psu (mm hr^{-1})$^{-1}$ (Table 1), which is consistent with the results presented by Boutin et al. (2016). In other words, the measurements of individual fresh layers made during SPURS-2 show a relationship between rain rate and vertical salinity gradient that is consistent with relationships developed with satellite-based measurements.

While Equation 1 assumes that ΔS_{max} depends only on R_{max}, Equation 2 describes ΔS_{max} as a function of both R_{max} and $\overline{U_{10}}$. It is evident from the SSP data that ΔS_{max} depends on both R_{max} and $\overline{U_{10}}$ (Figure 4b). Although these data exhibit significant variability, they demonstrate that the highest values of ΔS_{max} occur during rain events with higher R_{max} and smaller $\overline{U_{10}}$. A fit of Equation 2 to the data in Figure 4a,b gives values of k = 0.1 ± 0.2 psu (mm hr^{-1})$^{-1}$ and b = 1.0 ± 0.3 (Table 1). This fit is shown as dashed lines in Figure 4b. Though the uncertainty bounds (standard errors) of these coefficients are wide, the values are consistent with those found by Drushka et al. (2016) using output from one-dimensional modeling of idealized rain events. This suggests that although the rain events simulated with the one-dimensional model by Drushka et al. (2016) were idealized in terms of the temporal evolution of R and U_{10}, the modeled dependence of ΔS_{max} on R_{max} and $\overline{U_{10}}$ is similar to that found with field observations. This confirms that it is reasonable to use one-dimensional models to investigate the effect of rainfall on near-surface salinity.

Although the regression coefficients from fitting field data to Equation 2 are consistent with those found by Drushka

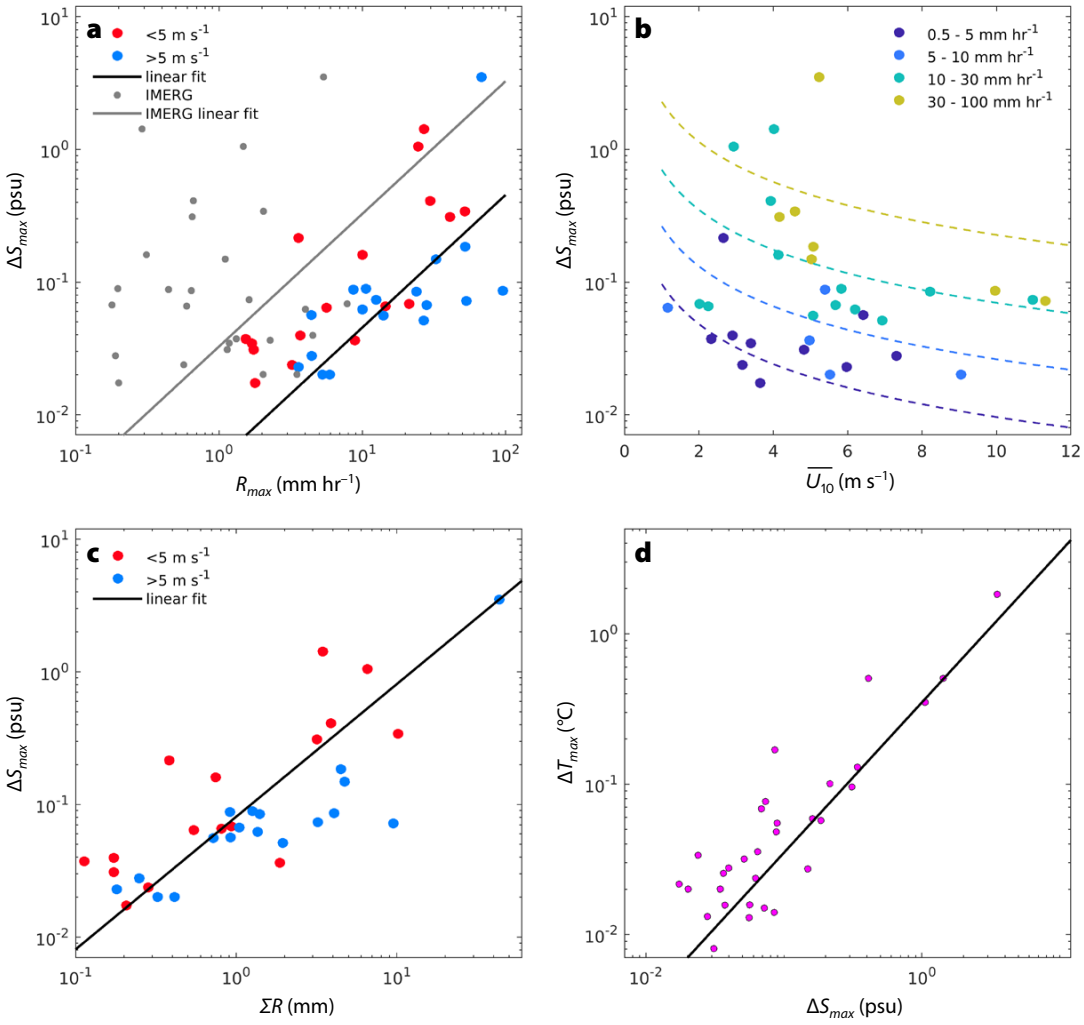

FIGURE 4. (a) ΔS_{max} plotted against R_{max} for each event. Colored dots show ship-based rain measurements, colored by $\overline{U_{10}}$. Gray dots show IMERG satellite-based rain measurements. The black and gray lines show linear fits to the ship-based and IMERG-based rain rates, respectively. (b) ΔS_{max} plotted against $\overline{U_{10}}$ for each event, colored by R_{max}. The thin dashed lines represent the fit of the data to Equation 2, evaluated at the midpoint value of R_{max} in each rain rate range. (c) ΔS_{max} plotted against ΣR for each event, colored by $\overline{U_{10}}$. The black line shows a linear fit to the data. (d) ΔT_{max} plotted against ΔS_{max} for each event. The black line shows a linear fit to the data.

et el. (2016), the scatter in Figure 4b suggests that factors other than R_{max} and $\overline{U_{10}}$ likely have significant impacts on ΔS_{max}. For instance, detailed inspection of the individual rain events captured with the SSP on a case-by-case basis reveals that the development of ΔS appears to be affected by horizontal advection in the upper ocean (current speeds were on average 0.3 m s^{-1}) and preexisting stratification from either diurnal warm layers or rain-generated fresh layers from previous rain events.

To evaluate the ability of accumulated rainfall to describe the strength of rain-formed vertical salinity gradients, Figure 4c shows ΔS_{max} plotted against ΣR. The r^2 value for the linear regression between ΔS_{max} and ΣR (i.e., replacing R_{max} with ΣR in Equation 1) is 0.77. This r^2 value is much larger than that for the fit between ΔS_{max} and R_{max} ($r^2 = 0.18$; Table 1), which indicates that ΣR is a better predictor of ΔS_{max} than R_{max} is. The fit between ΔS_{max} and ΣR using Equation 1 is also better than the fit of ΔS_{max} to ΣR and $\overline{U_{10}}$ using Equation 2, which has an r^2 value of 0.34 (Table 1). In other words, variability in ΔS_{max} can mostly be explained by variability in ΣR without considering U_{10}. This finding is counter-intuitive in light of the wind dependence that is seen in Figure 4a,b. We hypothesize that the variability of wind speed over the course of a rain event generates a time-variable and nonlinear forcing due to vertical mixing that is not well represented by an average value of wind speed. Thus, fitting ΔS_{max} to ΣR and $\overline{U_{10}}$ (Equation 2) degrades the fits in comparison to fitting ΔS_{max} only to ΣR (Equation 1). Alternatively, it may be that Equation 2 is not the correct model for the wind dependence of ΔS_{max}.

The close correlation between salinity and temperature variations during rain events (Figure 3c,d) was observed during all 35 rain events observed with the SSP. This is illustrated in Figure 4d, which shows a high correlation between ΔT_{max} and ΔS_{max}. A least-squares linear regression using data from the 35 events produces the relationship $\Delta T_{max} = (0.35 \pm 0.01°C\ psu^{-1})\ \Delta S_{max}$, and has an r^2 value of 0.89. This strong linear relationship is consistent with results from the prognostic model that was developed by Bellenger et al. (2016) to represent rain freshening and cooling.

Instantaneous Response of Upper-Ocean Salinity to Rain and Wind

In the two sections immediately above, individual rain events were isolated and quantified using ΔS_{max} and R_{max}. It is also useful to quantify the instantaneous relationship of ΔS with R and U_{10} at any given time. An instantaneous relationship may be particularly applicable to satellite data, which represent snapshots (e.g., of R, U_{10}, or $S_{0.01m}$) and thus may not capture the maximum R or minimum $S_{0.01m}$ for a given rain event. Here, we relate ΔS to R and U_{10} for all times that it was raining, without separating the data into discrete rain events. Figure 5a shows $\Delta S_{1.1-0.05m}$ for all data points having $R > 0.5$ mm hr^{-1} as a function of R, where the data point color denotes U_{10}. The dependence of $\Delta S_{1.1-0.05m}$ on both R and U_{10} is clear: $\Delta S_{1.1-0.05m}$ is positively correlated with R, with the largest $\Delta S_{1.1-0.05m}$ observed when U_{10} is low. This can be seen by binning $\Delta S_{1.1-0.05m}$ as a function of U_{10} and R (Figure 5b), which shows a clear correlation of $\Delta S_{1.1-0.05m}$ with R and U_{10} when $U_{10} < 7$ m s^{-1}. At higher wind speeds, $\Delta S_{1.1-0.05m}$ is small and no longer shows a dependence on R, suggesting that salinity gradients in the upper meter of the ocean are rarely seen for wind speeds greater than about 7 m s^{-1} (consistent with the observations of Thompson et al., 2019). Figure 5b demonstrates that the average salinity response in the upper 1 m of the ocean to rainfall is effectively instantaneous, with local rain and wind explaining much of the variability in $\Delta S_{1.1-0.05m}$. A fit of Equation 2 to all of the data shown in Figure 5a for $U_{10} < 8$ m s^{-1} gives the coefficients $k = 0.21 \pm 0.01$ (mm $hr^{-1})^{-1}$ and $b = 1.54 \pm 0.01$ (shown as thin dashed lines on Figure 5b). Thus, $\Delta S_{1.1-0.05m}$ observed by the SSP is linearly related to R and inversely proportional to U_{10} at any given time, consistent with ΔS_{max} for individual rain events (Figure 4b) and ΔS estimated with a one-dimensional model of idealized rain events (Drushka et al., 2016).

DISCUSSION AND CONCLUSIONS

During the 2016 and 2017 SPURS-2 cruises, the SSP measured vertical profiles of temperature and salinity from 0.05 m to 1.1 m and dissipation rate at 0.37 m depth for 35 distinct rain events.

TABLE 1. Parameters used in fitting observations to Equations 1 and 2, and resulting coefficients.

Depth Range for ΔS_{max}	Rain Data Set	Equation Used for Fit	Fit Coefficients	r^2
1.1–0.05 m	In situ R_{max} (mm hr^{-1})	Eq. 1	$k = 0.005 \pm 0.001$ psu (mm $hr^{-1})^{-1}$	0.18
1.1–0.05 m	R_{IMERG} (mm hr^{-1})	Eq. 1	$k = 0.03 \pm 0.02$ psu (mm $hr^{-1})^{-1}$	0.34
5–0.05 m	R_{IMERG} (mm hr^{-1})	Eq. 1	$k = 0.16 \pm 0.07$ psu (mm $hr^{-1})^{-1}$	0.44
1.1–0.05 m	In situ R_{max} (mm hr^{-1})	Eq. 2	$k = 0.1 \pm 0.2$ psu (mm $hr^{-1})^{-1}$ $b = 1.0 \pm 0.3$	0.22
1.1–0.05 m	In situ ΣR (mm)	Eq. 1 (with ΣR instead of R)	$k = 0.081 \pm 0.001$ psu mm^{-1}	0.77
1.1–0.05 m	In situ ΣR (mm)	Eq. 2 (with ΣR instead of R)	$k = 0.5 \pm 0.2$ psu mm^{-1} $b = 1.1 \pm 0.3$	0.34

These events represent 39 hours of data collected during a range of wind and rain conditions (Figure 2). The SSP measurements produced a rich data set that enables detailed characterization of the response of the upper meter of the ocean to rainfall. A major focus of this paper was to assess two parameterizations that have been developed to describe the vertical salinity gradients that form due to rainfall (Equations 1 and 2).

Equation 1 is a linear relationship between ΔS_{max} and R_{max} that was developed using satellite-based rain products and satellite/Argo salinities (Boutin et al., 2014, 2016). In situ rain rates measured from the ship were an order of magnitude greater than satellite-based rain rates from the IMERG product (Figure 4a). When this difference in R between IMERG and in situ is accounted for, and the depth range over which ΔS_{max} is computed is taken into account, the SSP-based regression coefficient between ΔS_{max} and R_{max} is in agreement with the results presented by Boutin et al. (2016). This result implies that applying or comparing parameterizations of near-surface salinity stratification due to rainfall requires careful consideration of the spatial and temporal scales used.

Fitting Equation 2 using R_{max} and $\overline{U_{10}}$ to the ΔS_{max} (Figure 4b) produced coefficients that, within the uncertainties, were consistent with the results from a one-dimensional modeling study of idealized rain events (Drushka et al., 2016). This agreement suggests that although the idealized rain events in the model oversimplified the atmospheric forcing on the ocean, the modeled response of the upper ocean to rainfall and wind compares reasonably well to that observed with the SSP. However, wide scatter in the data and large uncertainties on the fit to Equation 2 indicate that ΔS_{max} is not well described with a simple parameterization based on R_{max} and $\overline{U_{10}}$. Other factors, such as mixing from surface and internal waves, advection, and existing near-surface stratification also likely affect the vertical salinity gradients generated by rain. In addition, as described in the section on Sampling Considerations, sampling a constantly evolving rain field from a moving platform also likely confounds the temporal and spatial variability of the impact of rainfall on ΔS. It is thus unsurprising that ΔS_{max} cannot be perfectly described by R_{max} and $\overline{U_{10}}$.

Equations 1 and 2 were both developed using rain rate as a metric to describe ΔS_{max}. The data shown in Figure 4c demonstrate that the total accumulated rainfall for an event (ΣR) describes the strength of vertical salinity gradients better than the peak rain rate of an event (Table 1). This finding is in contrast to the results of the modeling study of Drushka et al. (2016), who found R_{max} to be a better predictor of ΔS_{max} than ΣR. This can be explained by the fact that the idealized rain events modeled by Drushka et al. (2016) were forced using constant U_{10} and a smooth time series of R with a single peak. Those forcing characteristics led the model to predict a single well-defined ΔS_{max} for each rain event. The situation is rarely so simple for real-world rain events, in which rainfall intensity varies on short timescales and small spatial scales. Rain accumulation thus explains more variability in ΔS_{max} than does R_{max}. Interestingly, regressing ΔS_{max} to ΣR

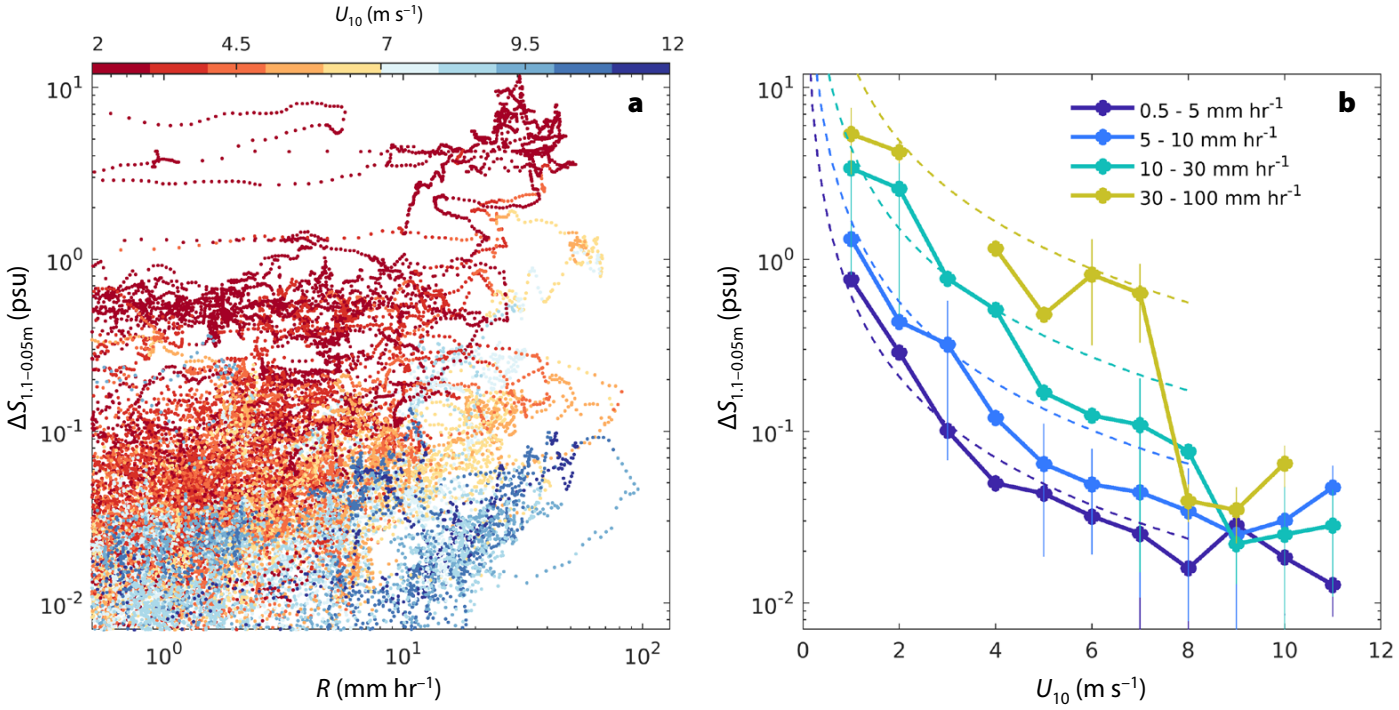

FIGURE 5. (a) $\Delta S_{1.1-0.05m}$ as a function of R for all data collected with the SSP while $R > 0.5$ mm hr^{-1}, where each data point has been colored by U_{10}. (b) $\Delta S_{1.1-0.05m}$ as a function of U_{10}, colored by R. Dots and thick lines represent the raw data shown in Figure 4a that have been binned by R and U_{10}. Thin dashed lines represent fit of Equation 2 to all raw data having $U_{10} < 8$ m s^{-1}, which gives $\Delta S_{1.1-0.05m} = 0.22 \cdot R \cdot U_{10}^{-1.6}$, evaluated at the midpoint value of R in each rain rate range.

alone produces a much better fit in comparison to including $\overline{U_{10}}$ in the fit, despite the clear dependence of ΔS on both wind speed and rain rate demonstrated in Figures 4b and 5b. We speculate that because wind speed varies significantly during the course of a single rain event, an average value of wind speed does not represent the nonlinear impacts of wind forcing on upper-ocean mixing and hence on ΔS. Including $\overline{U_{10}}$ thus degrades the fit of S_{max} to ΣR. In addition, Equation 2 may not be the best model to describe the wind speed and rain dependence of vertical salinity gradients. Unraveling the relative effects of time-variable rain, wind, and mixing on vertical salinity anomalies is beyond the scope of this paper and is left to future studies that combine modeling and analysis of the SSP data collected during SPURS-2.

By considering ΔS at any time as an instantaneous salinity response to local wind and rain forcing, Figure 5b demonstrates that ΔS is linearly related to R and inversely related to U_{10} (for $U_{10} < 8$ m s^{-1}). This is potentially valuable for using instantaneous measurement of R and U_{10} (e.g., from satellites or infrequent in situ measurements) to predict the presence of near-surface salinity stratification. The very high correlation between ΔT_{max} and ΔS_{max} (Figure 4d) has potential implications for using temperature as a proxy for salinity in order to study near-surface fresh layers. Near-surface temperature measurements (e.g., from satellites and surface drifters) are more prevalent than near-surface salinity measurements. If rain-induced cooling can be identified from temperature observations, and distinguished from cooling due to other causes (e.g., by matching to satellite rain observations), it may be possible to estimate rain-induced ΔS from ΔT measurements.

REFERENCES

Asher, W.E., A.T. Jessup, R. Branch, and D. Clark. 2014a. Observations of rain-induced near surface salinity anomalies. *Journal of Geophysical Research* 119:5,483–5,500, https://doi.org/10.1002/2014JC009954.

Asher, W.E., A.T. Jessup, and D. Clark. 2014b. Stable near-surface ocean salinity stratifications due to evaporation observed during STRASSE. *Journal of Geophysical Research* 119(5):3,219–3,233, https://doi.org/10.1002/2014JC009808.

Bellenger, H., K. Drushka, W. Asher, G. Reverdin, M. Katsumata, and M. Watanabe. 2016. Extension of the prognostic model of sea surface temperature to rain-induced cool and fresh lenses. *Journal of Geophysical Research* 122(1):484–507, https://doi.org/10.1002/2016JC012429.

Boutin, J., N. Martin, G. Reverdin, S. Morisset, X. Yin, L. Centurioni, and N. Reul. 2014. Sea surface salinity under rain cells: SMOS satellite and in situ drifters observations. *Journal of Geophysical Research* 119:5,533–5,545, https://doi.org/10.1002/2014JC010070.

Boutin, J., Y. Chao, W.E. Asher, T. Delcroix, R. Drucker, K. Drushka, N. Kolodziejczyk, T. Lee, N. Reul, G. Reverdin, and others. 2016. Satellite and in situ salinity: Understanding near-surface stratification and sub-footprint variability. *Bulletin of the American Meteorological Society* 97:1,391–1,407, https://doi.org/10.1175/BAMS-D-15-00032.1.

Clayson, C.A., J.B. Edson, A. Paget, R. Graham, and B. Greenwood. 2019. Effects of rainfall on the atmosphere and the ocean during SPURS-2. *Oceanography* 32(2):86–97, https://doi.org/10.5670/oceanog.2019.216.

Drucker, R., and S.C. Riser. 2014. Validation of Aquarius sea surface salinity with Argo: Analysis of error due to depth of measurement and vertical salinity stratification. *Journal of Geophysical Research* 119:4,626–4,637, https://doi.org/10.1002/2014JC010045.

Drushka, K., W.E. Asher, B. Ward, and K. Walesby. 2016. Understanding the formation and evolution of rain-formed fresh lenses at the ocean surface. *Journal of Geophysical Research* 121:2,673–2,689, https://doi.org/10.1002/2015JC011527.

Gosnell, R., C.W. Fairall, and P.J. Webster. 1995. The sensible heat of rainfall in the tropical ocean. *Journal of Geophysical Research* 100(C9):18,437–18,442, https://doi.org/10.1029/95JC01833.

Harrison, E.L., F. Veron, D.T. Ho, M.C. Reid, P. Orton, and W.R. McGillis. 2012. Nonlinear interaction between rain- and wind-induced air-water gas exchange. *Journal of Geophysical Research* 117(C3), https://doi.org/10.1029/2011JC007693.

Ho, D.T., C.J. Zappa, W.R. McGillis, L.F. Bliven, B. Ward, J.W. Dacey, P. Schlosser, and M.B. Hendricks. 2004. Influence of rain on air-sea gas exchange: Lessons from a model ocean. *Journal of Geophysical Research* 109(C8), https://doi.org/10.1029/2003JC001806.

Houze, R.A., Jr., K.L. Rasmussen, M.D. Zuluaga, and S.R. Brodzik. 2015. The variable nature of convection in the tropics and subtropics: A legacy of 16 years of the Tropical Rainfall Measuring Mission satellite. *Reviews of Geophysics* 53:994–1,021, https://doi.org/10.1002/2015RG000488.

Moulin, A.J., J.N. Moum, and E.L. Shroyer. 2018. Evolution of turbulence in the diurnal warm layer. *Journal of Physical Oceanography* 48:383–396, https://doi.org/10.1175/JPO-D-17-0170.1.

Price, J.F. 1979. Observations of a rain-formed mixed layer. *Journal of Physical Oceanography* 9(3):643–649, https://doi.org/10.1175/1520-0485(1979)009<0643:OOARFM>2.0.CO;2.

Santos-Garcia, A., M.M. Jacob, W.L. Jones, W.E. Asher, Y. Hejazin, H. Ebrahimi, and M. Rabolli. 2014. Investigation of rain effects on Aquarius sea surface salinity measurements. *Journal of Geophysical Research* 119(11):7,605–7,624, https://doi.org/10.1002/2014JC010137.

Soloviev, A., and R. Lukas. 1997. Observation of large diurnal warming events in the near-surface layer of the western equatorial Pacific warm pool. *Deep Sea Research Part I* 44(6):1,055–1,076, https://doi.org/10.1016/S0967-0637(96)00124-0.

Soloviev, A.V., S. Matt, and A. Fujimura. 2015. Three-dimensional dynamics of freshwater lenses in the ocean's near-surface layer. *Oceanography* 28(1):142–149, https://doi.org/10.5670/oceanog.2015.14.

Sun, Q., C. Miao, Q. Duan, H. Ashouri, S. Sorooshian, and K.-L. Hsu. 2018. A review of global precipitation data sets: Data sources, estimation, and intercomparisons. *Reviews of Geophysics* 56:79–107, https://doi.org/10.1002/2017RG000574.

ten Doeschate, A., G. Sutherland, H. Bellenger, S. Landwehr, L. Esters, and B. Ward. In press. Upper ocean response to rain observed from a vertical profiler. *Journal of Geophysical Research*, https://doi.org/10.1029/2018JC014060.

Thompson, E.J., J.N. Moum, C.W. Fairall, and S.A. Rutledge. 2019. Wind limits on rain layers and diurnal warm layers. *Journal of Geophysical Research* 124:897–924, https://doi.org/10.1029/2018JC014130.

Walesby, K., J. Vialard, P. Minnett, A. Callaghan, and B. Ward. 2015. Observations indicative of rain-induced double diffusion in the ocean surface boundary layer. *Geophysical Research Letters* 42:3,963–3,972, https://doi.org/10.1002/2015GL063506.

Wijesekera, H., C. Paulson, and A. Huyer. 1999. The effect of rainfall on the surface layer during a westerly wind burst in the western equatorial Pacific. *Journal of Physical Oceanography* 29(4):612–632, https://doi.org/10.1175/1520-0485(1999)029<0612:TEOROT>2.0.CO;2.

Zappa, C.J., D.T. Ho, W.R. McGillis, M.L. Banner, J.W. Dacey, L.F. Bliven, B. Ma, and J. Nystuen. 2009. Rain-induced turbulence and air-sea gas transfer. *Journal of Geophysical Research* 114(C7), https://doi.org/10.1029/2008JC005008.

ACKNOWLEDGMENTS

This work was supported by National Science Foundation grant OCE-1458759 and NASA grant NNX15AF68G. We thank Captains Curl and Murline and the crew of R/V *Revelle* for their assistance in carrying out the SPURS-2 field experiment. We also thank Trina Litchendorf and the science crew on the SPURS-2 cruises for assistance in deploying and recovering the SSP. Finally, we are grateful to two anonymous reviewers for their suggestions.

AUTHORS

Kyla Drushka (kdrushka@apl.uw.edu) is Principal Oceanographer, **William E. Asher** is Senior Principal Oceanographer, **Andrew T. Jessup** is Senior Principal Oceanographer, **Elizabeth J. Thompson** is Senior Meteorologist, **Suneil Iyer** is Graduate Research Student Assistant, and **Dan Clark** is Senior Engineer, all at the Applied Physics Laboratory, University of Washington, Seattle, WA, USA.

ARTICLE CITATION

Drushka, K., W.E. Asher, A.T. Jessup, E.J. Thompson, S. Iyer, and D. Clark. 2019. Capturing fresh layers with the surface salinity profiler. *Oceanography* 32(2):76–85, https://doi.org/10.5670/oceanog.2019.215.

COPYRIGHT & USAGE